Surface-Phonon Polariton Contribution to Nanoscale Radiative Heat Transfer.

Emmanuel Rousseau, Marine Laroche, Jean-Jacques Greffet

Surface-Phonon Polariton Contribution to Nanoscale Radiative Heat Transfer.

Emmanuel Rousseau*, Marine Laroche, and Jean-Jacques Greffet
Laboratoire Charles Fabry, Institut d'Optique
CNRS, Univ Paris-sud
Campus Polytechnique RD 128
91127 Palaiseau cedex, France

Heat transfer between two plates of polar materials at nanoscale distance is known to be enhanced by several orders of magnitude as compared with its far-field value. In this article, we show that nanoscale heat transfer is dominated by the coupling between surface phonon-polaritons located on each interface. Furthermore, we derive an asymptotic closed-form expression of the radiative heat transfer between two polar materials in the near-field regime. We study the temperature dependence of the heat transfer coefficient and we find that it differs markedly from the blackbody T^3 law. We show that the Surface-Phonon Polariton dominates the heat transfer for distances smaller than 50 nm. We extend asymptotic expressions up to 400 nm by taking into account other modes contributions. For temperatures smaller than 1500 K, the asymptotic expression yields the correct value of the heat transfer with an accuracy better than 20%.

I. INTRODUCTION

The heat flux between two bodies in a vacuum is only due to radiative heat transfer. This transfer can be enhanced by many orders of magnitude when the distance separating the bodies becomes smaller than the thermal wavelength $\lambda_T = \frac{\hbar c}{k_B T}$ where $\hbar$ is Planck's constant, k_B is Boltzman's constant, c is the light velocity and T is the temperature. This is due to energy tunneling mediated by evanescent waves with parallel wavevector to the interface larger than ω/c where ω is the circular frequency. Cravalho et al.[1] were the first to point out this role of the evanescent waves. However they considered only the case where evanescent waves in the gap result from frustrated total reflection of propagating waves in the material. Using the framework of fluctuational electrodynamics[2] the contribution of evanescent waves in the gap which results from electromagnetic modes with parallel wavevectors larger than $n\omega/c$ where n is the real part of the refractive index has been shown to play an important role[3–9]. These modes are called surface modes due to their confinement close to the interface. A quantum-mechanical derivation[10] has confirmed these results. Different geometries have been studied. The heat transfer between a particle and a surface has been investigated by several authors[11,12]. In the case of a metallic nanoparticle and a metallic surface it has been shown that magnetic energy plays a key role[19] leading to a saturation of the radiative heat transfer for distances smaller than the skin depth. More sophisticated geometries have also been studied in Ref.[15–17] and Ref.[18]. They are respectively devoted to the case of heat transfer between thin films or spheres. They mainly deal with surface modes contribution in theses geometries. The role of non-local effects in nanoscale thermal radiation has been studied in Ref.[13,14]. It was concluded that non-local effects have to be taken into accounts for distances smaller than 1 nm. Recent reviews can be found in Ref.[20–23].

Experimental investigations of this phenomenon started in the late 70's at cryogenic temperatures[24] and micrometric gaps[25]. Further attempts to measure a heat flux between metallic surfaces have proved to be inconclusive[26,27]. Recent experiments based on scanning microscopy techniques have reached the nanometric regime thereby enhancing the conductance. The effect was clearly observed although the lack of good control of the tip geometry did not allow quantitative comparison with theory[28,29]. The more recent experiments are performed using glass. It had been predicted theoretically that the heat flux between polar materials supporting surface phonon polaritons (SPP) should be enhanced by roughly an order of magnitude[8,12]. This is the case for polar materials such as silicon carbide SiC, quartz, silica, alumina. In the case of polar materials, the energy flux is important because the material resonance is close to the maximum of the Planck's spectrum i.e. in the infrared range. Surface phonon-polaritons are then thermally activated on the contrary to surface plasmon-polariton in metals whose resonant frequency lies in the U.V. Taking advantage of the large enhancement due to surface phonon-polariton, new data have been reported[30–32] for the flux between a sphere and a plane. Using the Derjaguin approximation and a numerically computed form of the heat transfer coefficient, it has been shown that the Polder theory can reproduce with great accuracy the experimental results[32]. Near-field heat transfer may be important for applications such as thermophotovoltaic devices[23,33] magnetic recording[34], local heating or heat assisted lithography.

In this paper, we report a detailed theoretical analysis of the heat transfer due to surface phonon polaritons between two semi-infinite bodies. We identify the contributions of the different electromagnetic modes and we find that the heat transfer is dominated by the surface-

*Electronic mail: emmanuel.rousseau@institutoptique.fr

phonon polariton contribution for gaps smaller than 50 nm. We are then able to derive a closed-form expression of the heat transfer coefficient with a distance dependence that varies as l^{-2} where l is the gap between the bodies. We also investigate its temperature dependence. We find that the T^3 blackbody law is no longer valid. Instead, the heat transfer coefficient decreases for temperatures above 1500 K. We extend the range of application of the analytical formula in including the contribution of other modes. We give an analytical formula which is valid for separation up to 400 nm.

II. DESCRIPTION AND MODELLING

A. Description of the system

The system under study consists in two infinite media separated by a vacuum gap l (see Fig:1). Their temperatures are supposed to be uniform and noted T and $T+\delta T$. We assume that the temperature difference is small so that we can linearize the flux and introduce a heat transfer coefficient $h_{tot}(l,T)$ defined as:

$$\varphi(l,T) = h_{tot}(l,T)\delta T \tag{1}$$

where $\varphi(l,T)$ is the radiative flux, T the temperature of the first plate, $T+\delta T$ the temperature of the second plate (see Fig. 1).

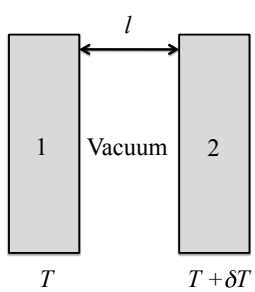

FIG. 1: Two semi-infinite half-spaces separated by a vacuum gap (distance l).

As previously seen, optical properties affect heat transfer[8,37]. We will use silicon carbide to illustrate our results because its optical properties are well-known and well-described by a simple model. Only four parameters are needed: the dielectric function at high frequency ε_∞, the longitudinal and the transverse optical-phonon frequency (ω_{LO} and ω_{TO} respectively) and a damping factor Γ.

$$\varepsilon(\omega) = \varepsilon_\infty\left(\frac{\omega_{LO}^2 - \omega^2 - i\Gamma\omega}{\omega_{TO}^2 - \omega^2 - i\Gamma\omega}\right)$$

Moreover, these four parameters have been measured[35] at five different temperatures in the range [300-800K]. The high-frequency dielectric function ε_∞ and the optical-phonon frequencies ω_{TO} and ω_{LO} change by less than 2% and will be taken to be constant. On the other hand, the damping factor increases linearly with temperature. The fit parameters are: $\Gamma(T) = 4.8329 + 0.0183(T-300)\ cm^{-2}$. Note that this linear fit yields a value at 300K $\Gamma(300K) = 4.8329\ cm^{-2}$ that differs by 1.5% from the tabulated value ($4.76\ cm^{-2}$) in Ref.[36].

B. Theory

Computing radiative heat transfer in the presence of evanescent waves requires a complete electromagnetic treatment[3,5] in the framework of fluctuational electrodynamics[4] introduced by Rytov. The flux is obtained by calculating the Poynting vector across the gap separating the two bodies as shown in refs[7,8,21,22]:

$$h_{tot}(l,T) = \sum_{i=s,p}\int_0^\infty d\omega[h^i_{prop}(l,T,\omega) + h^i_{evan}(l,T,\omega)] \tag{2}$$

where the sum over $i = s\ (TE), p\ (TM)$ accounts for the two polarizations. We have introduced the contribution of the propagating modes:

$$h^{s,p}_{prop}(l,T,\omega) = h^0(\omega,T)\times \int_0^{k_0}\frac{\kappa d\kappa}{k_0^2}\frac{(1-|r^{s,p}_{31}|^2)(1-|r^{s,p}_{32}|^2)}{|1-r^{s,p}_{31}r^{s,p}_{32}e^{-2i\gamma l}|^2}$$

and the contribution of the evanescent modes:

$$h^{s,p}_{evan}(l,T,\omega) = h^0(\omega,T)\times \int_{k_0}^\infty\frac{\kappa d\kappa}{k_0^2}\frac{4Im(r^{s,p}_{31})Im(r^{s,p}_{32})}{|1-r^{s,p}_{31}r^{s,p}_{32}e^{-2\gamma'' l}|^2}e^{-2\gamma'' l}, \tag{3}$$

where $h^0(\omega,T)$ is the derivative of the blackbody intensity:

$$h^0(\omega,T) = \pi\frac{\partial L^0}{\partial T}(\omega,T) = \frac{1}{T}\frac{\hbar\omega}{k_bT}\frac{\hbar\omega^3}{4\pi^2c^2}\frac{1}{[2\sinh(\frac{\hbar\omega_0}{2k_bT})]^2}.$$

$r^{s,p}_{31}$ and $r^{s,p}_{32}$ are the Fresnel coefficient of each interface (3 denotes the vacuum) and are given in the appendix. The Fresnel coefficients depend on the polarisation s or p of the incident wave.

$\gamma'' = Im[\gamma]$ is the imaginary part of the z-component of the wave vector in the vacuum gap $\gamma = \sqrt{(\omega/c)^2 - \kappa^2}$ whereas κ is the component parallel to the interface. They satisfy the relation: $\kappa^2 + \gamma^2 = (\omega/c)^2$ where ω is the angular frequency and c the speed of light. We also define $k_0 = \omega/c$.

The dependence of the heat transfer coefficient for two slabs of SiC as a function of the gap distance is shown in Fig. 2. It represents the total heat transfer coefficient, its

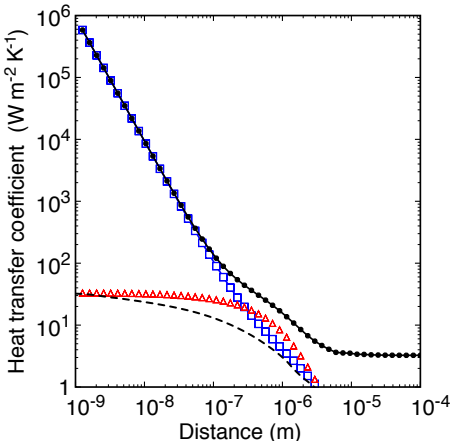

FIG. 2: Evolution of the heat transfer coefficient with distance. Black dots curve: Total heat transfer coefficient (h_{tot}). Red triangles curve: Evanescent s-polarized contribution (h^s_{evan}). Blue square curve: Evanescent p-polarized (h^p_{evan}). Black dashed line: Contribution of p-polarized evanescent waves coming from frustrated reflections. The average temperature is the room temperature (T=300 K). Colors are available online.

evanescent p- and s-polarized component versus the gap distance l. We can distinguished three regimes: 1) For gaps smaller than $\lambda_T/50$ (*i.e.* $100nm$ at room temperature), the heat transfer is mainly dominated by the p-polarized evanescent waves contribution. 2)Between 100 nm and 400 nm there is an intermediate regime where both s- and p-polarized contribution have to be taken into account. 3) For a distance larger than λ_T (i.e. 10 μm at room temperature), the heat transfer coefficient is independent of the distance when the propagating part of equation (2) dominates the heat transfer.

III. ASYMPTOTIC EXPRESSIONS FOR EXTREME NEAR-FIELD REGIME

In this section we focus on the regime where the p-polarization dominates the heat transfer i.e. for gaps smaller than $\lambda_T/50$.

In this extreme near-field regime, the heat transfer coefficient reduces to:

$$h^p_{evan}(l,T) \simeq \int_0^\infty d\omega h^p_{evan}(l,T,\omega) \qquad (4)$$

In order to compute the radiative heat transfer in the asymptotic regime, one has to integrate over the (ω,κ)-plane in order to account for all electromagnetic modes. We plot in Fig.3 the logarithm of the integrand of equation (4). From curve Fig.3-a, it is seen that four regions mainly contribute to the heat transfer. Note that the x-axis of Fig.3-a is in linear scale whereas the y-axis is in logarithm scale. Regions I and II correspond to waves which are propagating in the material and evanescent in the gap. Their contribution to the heat transfer coefficient is plotted Fig. 2 as the black dashed line. Regions III and IV correspond to the SPP contribution. In the extreme near-field regime, Fig.3-a and Fig.2 show that the SPP gives the leading contribution.

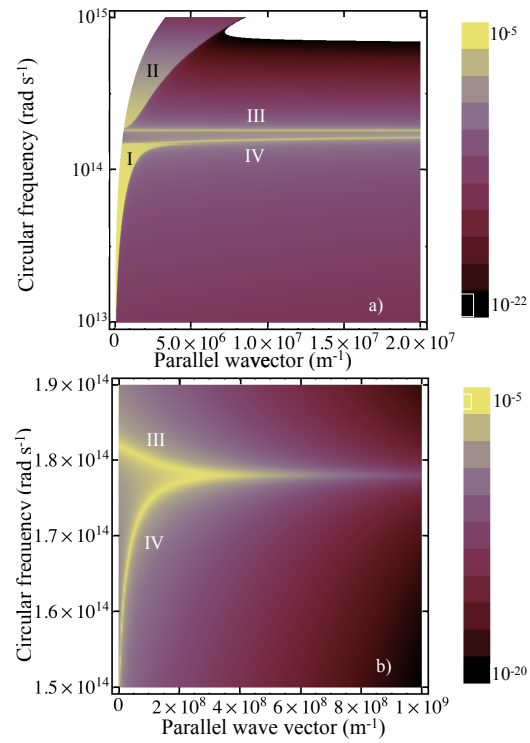

FIG. 3: Logarithm of the integrand of equation (4). Figure a) shows all the relevant scale. Four regions dominate the heat transfer coefficient. Region I and II render contribution of frustrated total internal reflection. Region III and IV correspond to the contribution of the surface-phonon polariton. Figure b) is a zoom on the surface mode contribution. It focus on a restrict frequency range but extend in a wider wave vector range. Note now that scales are linear. The region I and II contribution is no more visible because they are restrict to a narrow range of parallel wave vectors. The temperature is T=300 K and the gap l=10 nm.

A. Contribution of the Coupled SPP modes.

We now analyse the origin of the two narrow lines III and IV in Fig.3-a. A zoom on a narrow frequency region is shown in Fig.3-b using a linear scale. Let us consider the dispersion relation of the surface phonon-polaritons in the double interface geometry[38]. It is given by the solutions of equation (5):

$$r_p(\omega,\kappa)e^{-\gamma'' l} = \pm 1 \qquad (5)$$

In the electrostatic limit $\gamma'' \simeq \kappa$, the reflection factor takes the limiting form $\tilde{r}_p(\omega) = (\varepsilon(\omega)-1)/(\varepsilon(\omega)+1)$. An analytical solution of equation (5) can be derived:

$$\omega_-(\kappa) = \sqrt{\frac{\omega_{spp} - a\omega_{ch}e^{-\kappa l}}{1 - ae^{-\kappa l}}} \qquad (6)$$

$$\omega_+(\kappa) = \sqrt{\frac{\omega_{spp} + a\omega_{ch}e^{-\kappa l}}{1 + ae^{-\kappa l}}}$$

with $a = \frac{\varepsilon_\infty - 1}{\varepsilon_\infty + 1}$, $\omega_{spp} = \sqrt{\frac{\varepsilon_\infty \omega_l + \omega_t}{\epsilon_\infty + 1}}$ the one-interface surface-phonon frequency and $\omega_{ch} = \sqrt{\frac{\varepsilon_\infty \omega_l - \omega_t}{\epsilon_\infty - 1}}$ the Christiansen frequency. For κ larger than $1/l$, ω_+ and ω_- converge to the one-interface phonon-polariton frequency ω_{spp} which is the solution of $Re[\varepsilon(\omega)] = -1$.

The dispersion relation is plotted in Fig.4. It reproduces the two narrow lines of the integrand of equation (4-b). The dashed black line in Fig. 4 is the phonon-polariton frequency in the one-interface geometry. The asymptotic role of surface phonon-polariton has also been shown in the case of Casimir force[39]. These authors showed that the overlapping of the two surface phonon-polaritons leads to a symmetric (solution +) and an antisymmetric mode (solution −). For parallel wave vectors larger than $\kappa \gtrsim 5/l$, the overlapping and hence, the interaction between the two surface modes decrease. The frequency splitting is reduced so that the two lines merge. As seen in Fig.3-b this low interaction results in a weak contribution to the energy flux.

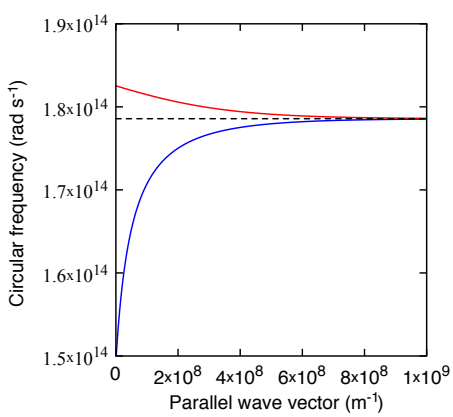

FIG. 4: Dispersion relation in the two interface geometry. This curve shows the phonon-polariton dispersion relation in the double interface geometry. The blue curve is the dispersion relation for the symmetric case whereas the red curve is the dispersion relation in the antisymmetric mode. They converge to the one-interface dispersion relation (dashed black line) for large parallel wave vectors. The gap between the two slabs is $l = 10nm$

B. Closed-form expression of the heat transfer coefficient

We now turn to the calculation of the surface-mode contribution to the heat transfer coefficient in the near-field regime. First, we rewrite equation (4) with new units: $u = \hbar\omega/k_BT$, $\tilde{\kappa} = \kappa/k_0$, $\tilde{\gamma} = k_0\sqrt{\tilde{\kappa}^2 - 1}$, $k_T = 1/\lambda_T$:

$$h^p_{evan}(l,T) = \int_0^\infty du h^p_{evan}(l,T,u)$$

with

$$h^p_{evan}(u,l,T) = 4\sigma T^3 \frac{15}{4\pi^4} h^0(u) \times \int_0^\infty \tilde{\gamma} d\tilde{\gamma} \frac{4Im(r_{31})Im(r_{32})e^{-2k_T\tilde{\gamma}ul}}{|1 - r_{31}r_{32}e^{-2k_T\tilde{\gamma}ul}|^2} \qquad (7)$$

where σ is the Stefan-Boltzmann constant.

Note that Fresnel coefficients are now function of u and $\tilde{\kappa}$ and $h^0(u) = u^4e^u/(e^u - 1)^2$. One can note that for evanescent waves:

$$\frac{Im(r_{31}r_{32})}{|1 - r_{31}r_{32}e^{-2k_T\tilde{\gamma}ul}|^2} e^{-2k_T\tilde{\gamma}ul} = Im[\frac{r_{31}r_{32}e^{-2k_T\tilde{\gamma}ul}}{1 - r_{31}r_{32}e^{-2k_T\tilde{\gamma}ul}}]$$

This allows to obtain an analytical form of (7) by removing the modulus function. In the electrostatic regime, the Fresnel coefficients are independent of the parallel wave vector $\tilde{\kappa}$: $\tilde{r}_p = \frac{\varepsilon(u)-1}{\varepsilon(u)+1}$. A final change of variable $X = 2\tilde{\gamma}k_Tul$ leads us to compute the surface-phonon Polariton contribution noted h_{spp}:

$$h_{spp}(u,l,T) = \frac{4\sigma T^3}{(k_Tl)^2} \frac{15}{3\pi^4} \frac{h^0(u)}{u^2} \times \frac{Im(\tilde{r}_{31})Im(\tilde{r}_{32})}{Im(\tilde{r}_{31}\tilde{r}_{32})} \int_0^\infty XdXIm[\frac{\tilde{r}_{31}\tilde{r}_{32}e^{-X}}{1 - \tilde{r}_{31}\tilde{r}_{32}e^{-X}}] \qquad (8)$$

The distance dependence ($h_{spp}(u,l,T) \propto 1/l^2$) is a consequence of the electrostatic limit and equation (8) can be integrated with the help of the polylogarithm function of the second order[40]:

$$h_{spp}(u,l,T) = \frac{4\sigma T^3}{(k_Tl)^2} \frac{15}{3\pi^4} \frac{h^0(u)}{u^2} \times \frac{Im(\tilde{r}_{31})Im(\tilde{r}_{32})}{Im(\tilde{r}_{31}\tilde{r}_{32})} Im[Li_2(\tilde{r}_{31}\tilde{r}_{32})] \qquad (9)$$

This is one of the key result of the paper. No assumptions have been made on the form of the Fresnel coefficients except that they are taken in the electrostatic limit where they are independent of the parallel wave vector.

We now compare the surface mode contribution $h_{spp}(\omega,l,T)$ (eq.9) and a numerical integration of the p-polarisation heat transfer coefficient $h^p_{evan}(\omega,l,T)$ as a function of the frequency ω.

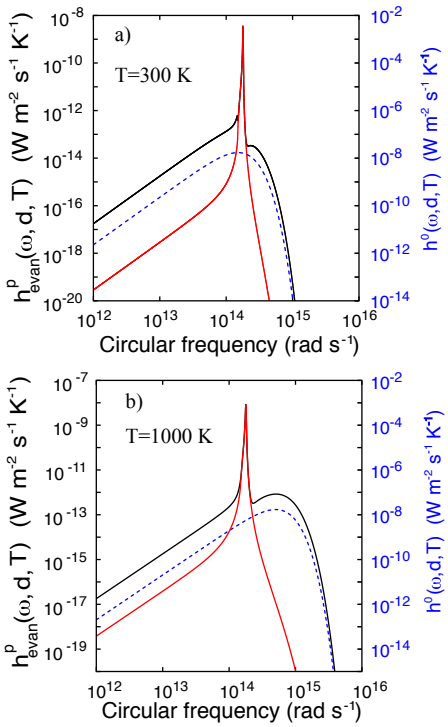

FIG. 5: Evolution of the monochromatic heat transfer coefficient for two different temperatures T=300 K (a) and T=1000 K (b). The gap is l=10 nm. We represent only the p-polarization component. The black curve is the exact numerical result and the red line is the asymptotic expression (equation 9). The dashed blue line is the derivative of the Planck function $h^0(\omega, T)$.

The comparison is done for two temperatures in Fig.5 and three distances in Fig.6. The black curve is a numerical integration of eq. (3). It describes only the contribution of the p-polarization. The red curves describe the asymptotic expressions (Eq. (3)) and the blue dashed curves are the derivative of the Planck function $h^0(\omega, T)$. The surface mode contribution describes correctly the peak for a large range of distances ($l \leq 1\mu m$) and temperatures ($T \leq 1500K$).

For distances smaller than 5 nm, the heat transfer is completely dominated by the surface mode which contributes for more than 99.5% to the total heat transfer at 300K. On the contrary at 100 nm only 48 % of the total flux is due to the surface-phonon polariton coupling. Actually, the closed-form expression fails to describe the total curve and underestimates the contribution of the low and high frequency modes. These modes follow the Planck function as it can be seen on Fig. 5-a and 5-b by considering the black and dashed blue curves at low and high frequencies.

Fig.6 shows that the peak amplitude varies as l^{-2}. On the contrary to surface mode contribution, the shape of the curve depends weakly on the distance l. The black curve level remains almost the same whereas the distance decreases. It will be shown that these modes result from

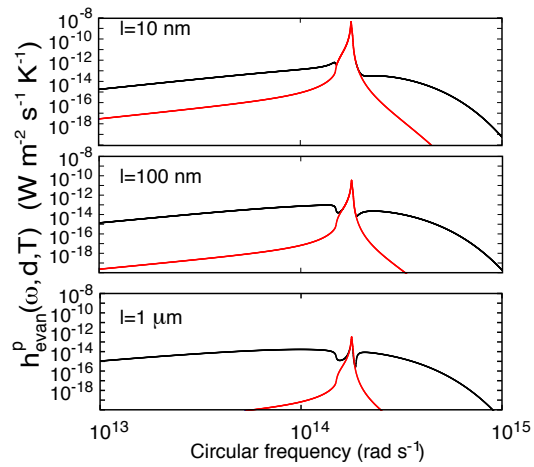

FIG. 6: Evolution of the monochromatic heat transfer coefficient for three different distances $l = 1\ \mu m$,$l = 100\ nm$, $l = 10\ nm$. We represent only the p-polarization component. The black curve is the exact numerical result and the red line is the surface phonon-polariton contribution (equation 9).The temperature is $T = 300\ K$.

frustrated reflection. Their contribution is analyzed in section IV.

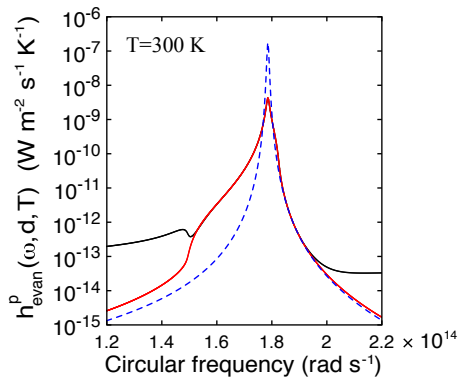

FIG. 7: Evolution of the p-polarization of the monochromatic heat transfer coefficient at T=300 K. The gap is l=10 nm. Black curve: p-polarization contribution to the monochromatic heat transfer coefficient obtained by a numerical integration of $h^p_{evan}(\omega, d, T)$ (eq.3). This is the exact result. Red curve: Contribution to the surface mode $h_{spp}(\omega, d, T)$. The dashed blue line is a rough estimate from Ref.[5,8].

We now focus (Fig.7) on the peak seen in Figures 5-a, 5-b, 6. The dashed blue line is a rough asymptotic estimate of the heat transfer coefficient derived in Ref.[5,8]. While it reproduces correctly the distance dependance ($h \propto 1/l^2$) and the order of magnitude of the heat transfer, this expression does not yield the correct amplitude and the correct width of the heat transfer coefficient. This is due to the fact that the actual dispersion relation of SPP in a gap had not been taken into account. Finally, let us emphasize that the closed-form expression

applies for all polar materials in a plane-plane geometry with similar or different materials.

C. Dependence of the near-field regime on the temperature

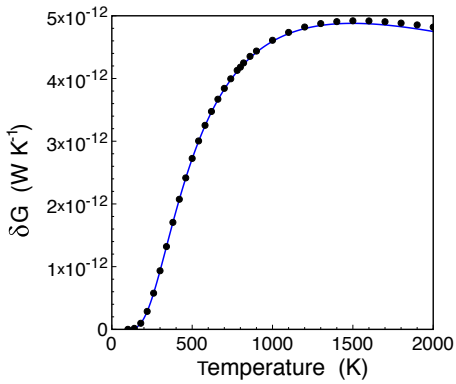

FIG. 8: Evolution of δG with temperature. The black dots result from the exact calculation whereas the blue line is the numerical integration of the asymptotic expression (i.e. equation (11)). Note that is crucial to use the temperature-dependent optical properties to compute δG

In this section, we shall investigate the dependence of the near-field heat transfer versus temperature. Since we could not integrate equation (9) over the reduced frequency u analytically, we performed a numerical integration and compared it with the exact results. To this aim, we define $\delta G(T)$ as:

$$h_{spp}(l,T) = \frac{\delta G(T)}{l^2} \tag{10}$$

with

$$\delta G(T) = \frac{4\sigma T^3}{k_T^2}\,\frac{15}{3\pi^4}\times \int_0^\infty du \frac{h^0(u)}{u^2}\frac{Im(\tilde{r}_{31})Im(\tilde{r}_{32})}{Im(\tilde{r}_{31}\tilde{r}_{32})} Im[Li_2(\tilde{r}_{31}\tilde{r}_{32})] \tag{11}$$

$\delta G(T)$ is shown in Fig. 8. The black dots are extracted from the exact numerical results whereas the blue curve results from the numerical integration of equation (11). The two curves perfectly fit for temperatures lower than 1500 K. It is clearly seen that $\delta G(T)$ presents a maximum for $T \simeq 1500K$. This temperature behaviour differs drastically from the black body. For a blackbody, the flux always increases with increasing T because the number of modes thermally activated increases.

A small discrepancy appears at high temperature. It can be attributed to the failure of the electrostatic limit. High frequency modes are activated by the Planck function and condition $\kappa \geq \omega/c$ cannot be satisfied anymore.

IV. ASYMPTOTIC EXPRESSIONS FOR THE INTERMEDIATE NEAR-FIELD REGIME.

As already mentionned, at room temperature the surface-phonon polariton dominates the heat transfer for distances smaller than 50 nm. In order to describe the heat transfer coefficient in a wider range of gaps one has to include the other modes contribution. In this section, we analyse the contribution of the evanescent waves coming from total internal reflection and find an asymptotic expression describing their contribution.

A. Contribution of Evanescent waves coming from frustated total internal reflection.

Some of the other modes are p-polarized waves coming from frustrated internal reflection at the interface. They correspond to regions I and II in Fig.3. Other modes are s-polarized evanescent waves which also come from total reflection.

All those modes are characterized by a parallel wave vector that satisfies: $k_0 \leq \kappa \leq n(\omega)k_0$ where $n(\omega)$ is the refractive index and k_0 denotes ω/c. Note that the refractive index depends on the circular frequency. As already noticed by Chapuis et al[14], those modes are bound by a maximal wave vector $\kappa_{max}(\omega) = \sqrt{|\varepsilon(\omega)|}k_0$ which gives rise to a saturation of the heat transfer coefficient as the distance decreases.

We plot in Fig.2 the contribution of total frustrated reflection in p (dashed black line) and s-polarization (red triangles). Both curves saturate and reach the same value at small gap. Note that the s-component reaches its saturation value for gaps larger than the p-component which saturates at extremely small gaps $l \simeq 1$ nm. As a consequence, the contribution due to s-polarization always dominates the heat transfer due to frustrated total internal reflection.

B. Closed-form expression of the s-polarized contribution to heat transfer in the saturation regime

Let us estimate the value of the heat transfer coefficient in the saturation regime. Following Pendry[6], we can use an upper bound given by:

$$A_s = \frac{4Im(r_s)^2 e^{-2\gamma'' d}}{|1 - r_s^2 e^{-2\gamma'' d}|^2} \leq 1$$

The saturation can thus be calculated by using the upper bound of A_s and integrating over the whole spectrum:

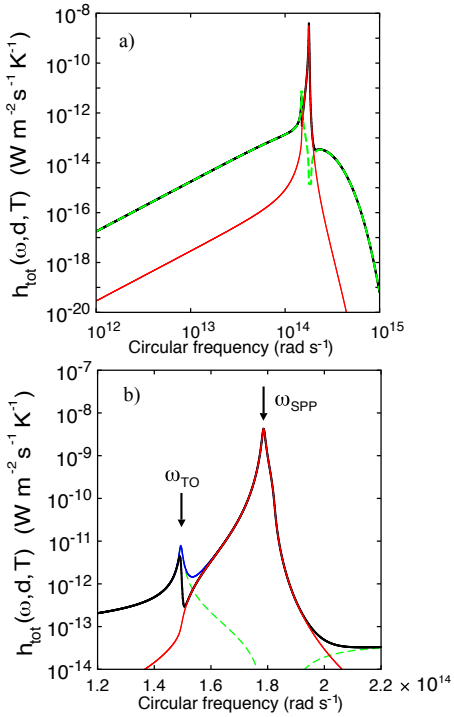

FIG. 9: Evolution of the total monochromatic heat transfer coefficient with circular frequency. The gap is l=10 nm and the temperature is $T = 300\ K$. a) The black curve is the total monochromatic heat transfer coefficient (polarization s+p). It is the result obtained from a numerical integration of eq. (3). The red line is the surface mode contribution $h_{spp}(\omega, d, T)$ (equation 9). The dashed green line is the contribution of the s-polarization in the saturation regime given by eq. 13. b) is a zoom in a narrow frequency range. The blue curve is the sum of $h_{sat}(\omega, d, T)$ and $h_{spp}(\omega, d, T)$.

$$h^{s,p}_{sat}(T) = \int_0^\infty d\omega h^0(\omega) \int_{k_0}^{\kappa_{max}=\sqrt{|\varepsilon(\omega)|}k_0} \frac{\kappa d\kappa}{k_0^2}$$
$$h^{s,p}_{sat}(T) = \int_0^\infty d\omega h^0(\omega) \frac{|\varepsilon(\omega)|-1}{2} \qquad (12)$$

This estimate holds for evanescent s- and p-polarized waves but as already noted the p-component is negligible for distance larger than 1 nm so we will deal only with the s-polarization in the following. We define the saturation monochromatic heat transfer coefficient as:

$$h_{sat}(\omega, T) = h^0(\omega) \frac{|\varepsilon(\omega)|-1}{2} \qquad (13)$$

We plot in Fig.9-a the monochromatic total heat transfer coefficient (polarization s+p) $h_{tot}(\omega, d, T)$ (eq.3) obtained from exact numerical results versus the frequency. We also plot the surface mode contribution $h_{spp}(\omega, d, T)$ (eq.9) and the saturation $h_{sat}(\omega, T)$ (eq.13). The sum of $h_{spp}(\omega, d, T)$ and $h_{sat}(\omega, T)$ now completely describes the exact numerical result. The shape and the peak are perfectly reproduced.

We now focus on the peak in Fig.9-b. There are actually two peaks. One at ω_{spp} due to the surface-phonon polariton frequency and described by the surface mode contribution $h_{spp}(\omega, T)$ as previously discussed. A small peak appears at ω_{TO}. It results from the resonant behaviour of the dielectric constant when frequencies approach ω_{TO}. This resonance induces a peak in the total monochromatic heat transfer. On the contrary to the surface-phonon polariton peak, this peak amplitude depends smoothly on the distance. Note nevertheless that at one micrometer this peak is no longer visible but its amplitude is independent on the distance for gap lower than $d \leq 100\ nm$. The expression $h_{sat}(\omega, T)$ accounts for this contribution.

The sum of $h_{sat}(\omega, T)$ and $h_{spp}(\omega, T)$ (blue curve Fig.9-b) slightly overestimates the contribution of modes lying in the window $[\omega_{TO}, \omega_{spp}]$ but perfectly fit to the exact result in the rest of the spectrum.

V. VALIDITY RANGE.

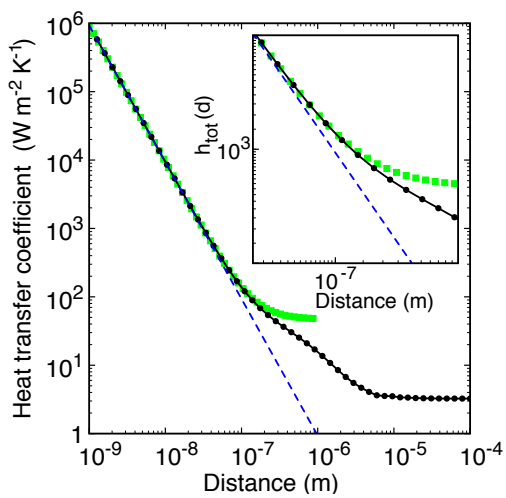

FIG. 10: Evolution of the total heat transfer coefficient with distance. Black dots curve: Total heat transfer coefficient (h_{tot}). Blue dashed curve: Contribution of the coupled surface-phonon polariton ($h^p_{spp}(d, T)$). The green squares curve is the approximate expression (h_{approx}) i.e. the sum of the dashed blue curve (h^p_{spp}) and the saturation of the s-polarization contribution (h^s_{sat}). The insert is a zoom on a restricted gap range. The average temperature is the room temperature (T=300 K). Colors are available online.

We now investigate the accuracy of the different asymptotic expressions and examine their validity range. We define the approximate heat transfer coefficient as the sum of the surface-phonon polariton contribution and the s-polarized contribution in the saturation regime :

$$h_{approx}(d,T) = h^p_{spp}(d,T) + h^s_{sat}(T)$$

where $h^p_{spp}(d,T)$ and $h^s_{sat}(d,T)$ result from numerical integration over the spectrum of the two closed-form expressions given by eq.(9) and eq.(12) respectively. The approximate coefficient is compared with the exact numerical results in the Fig.10 at room temperature for different distances. The insert is a zoom on a narrow distance range. The dashed blue curve is the contribution of the coupled surface-phonon polariton $h_{spp}(d,T)$. We added the saturation h^s_{sat} as the contribution of the s-polarization. The contribution of p-polarized evanescent waves coming from frustrated reflection is not added because it only plays a role at very small distance (below 1nm) as it can be seen Fig.10. With this procedure, the total heat transfer coefficient is well-described for distances up to 400 nm. As an example, the relative difference between the exact numerical result and the surface phonon contribution is 52% at $d = 100\ nm$ whereas it is only 2% with the approximate $h_{approx}(d,T)$.

Fig. 11 shows the relative difference between the total heat transfer h_{tot} and the approximation for temperature varying between [200-900 K] and gaps varying between $[10^{-9}, 10^{-6}\ m]$. The relative difference (R) is in percent: $R = 100 \times \frac{|h_{tot}(l,T) - h_{approx}(l,T)|}{h_{tot}(l,T)}$.

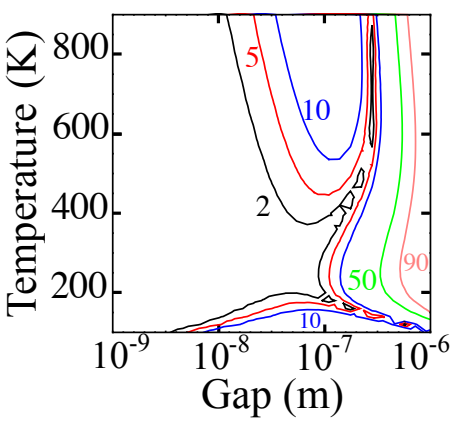

FIG. 11: Relative difference between the total heat transfer $h_{tot}(d,T)$ coefficient and the approximation $h_{approx}(d,T)$. Numbers indicate the relative difference (in percent).

VI. CONCLUSION

In this paper, we have shown that radiative heat transfer mainly results from the coupling of surface phonon-polariton for distances shorter than 50 nm. A careful analysis of their contribution allowed to derive a closed-form expression of the heat transfer coefficient. It can be cast in the form $\varphi(l,T) = \frac{\delta G(T)}{l^2} S\delta T$. We have investigated the temperature dependence of δG and we have found a behaviour markedly different from the blackbody radiation case. For distances larger than 50 nm, other contributions must be included. We derived a closed-form expression of the contribution of the s-polarized waves. This yields an analytical formula valid for distances up to 400 nm at room temperature. In summary, the results presented in this paper clarify the physical origin of the different contributions to the nanoscale heat transfer and provides closed-form expressions to compute quantitatively nanoscale heat transfer between polar materials.

The authors acknowledge the support of *Agence Nationale de la Recherche* through *Monaco* projects (ANR-06-NANO-062) and Leti-Carnot Institute.

VII. APPENDIX

The optical properties of the interface is included in the Fresnel reflection factors. Their explicit form is given below:

for the s-polarization:

$$r^s_{31} = \frac{\gamma - \gamma_1}{\gamma + \gamma_1}$$

with $\gamma = \sqrt{(\omega/c)^2 - \kappa^2}$ the z-component of wave vector in the vacuum and $\gamma_1 = \sqrt{\varepsilon_1(\omega/c)^2 - \kappa^2}$ the z-component of the wave vector in the material 1.

and for the p-polarization:

$$r^p_{31} = \frac{\varepsilon_1\gamma - \gamma_1}{\varepsilon_1\gamma + \gamma_1}$$

[1] E. G. Cravalho, C. L. Tien and R. P. caren, J. Heat Transfer **89**, 351 (1967).
[2] Rytov, S. M., Y. A. Kravtsov, and V. I. Tatarskii, Principles of Statistical Radiophyics (Springer, New York,1989), Vol. 3.
[3] D. Polder and M. Van Hove, Phys. Rev. B **4**, 3303 (1971).
[4] M.L. Levin, V. G. Polevoy and S. M. Rytov, Zh. Eksp. Teor. Fiz. **79**, 2087 (1980) [Sov. Phys. JETP **52**, 1054 (1980)]
[5] J. J. Loomis and H. J. Maris, Phys. Rev. B **50**, 18517 (1994).
[6] J. B. Pendry, J. Phys.: Condens. **11**, 6621-6633 (1999).
[7] A.I. Volokitin and B.N.J. Persson, Phys. Rev. B **63**, 205404 (2001).
[8] J-P. Mulet, K. Joulain, R. Carminati and J-J. Greffet, Microscale Thermophysical Engineering **6**, 209 (2002).
[9] S.Basu and Z. Zhang, Journ. Appl. Phys. **105**, 093535 (2009).
[10] M. Janowicz, D. Reddig, M. Holthaus, Phys. Rev. A **68**, 043823 (2003).

[11] I. Dorofeyev, J.Phys.D: Appl.Phys.**31** 600 (1998).
[12] J.P. Mulet, K. Joulain, R. Carminati, J.J. Greffet, Appl.Phys.Lett. **78**, 2931 (2001).
[13] I. Dorofeyev, Phys.Lett.A **372**, 1341 (2008).
[14] P.-O. Chapuis, S. Volz, C. Henkel, K. Joulain and J-J. Greffet, Phys. Rev. B **77**, 035431 (2008).
[15] M. Francoeur, M.P. Menguc, R. Vaillon, Appl. Phys. Lett. **93** 043109 (2008).
[16] S.A. Biehs Eur. Phys. J. B **58**, 423 (2007).
[17] Ph. Ben-Abdallah, Karl Joulain, Jrmie Drevillon, and Gilberto Domingues J. Appl. Phys. 106, 044306 (2009).
[18] A. Narayanaswamy and G. Chen, Phys. Rev. B **77** , 075125 (2008).
[19] P.O. Chapuis, M. Laroche, S. Volz, J.J. Greffet, Phys.Rev.B **77**, 125402 (2008).
[20] E. A. Vinogradov, I. A. Dorofeyev, Physics-Uspekhi **52**, 425 (2009).
[21] A.I. Volokitin and B.N.J. Persson, Rev. Mod. Phys. **79**, 1291 (2007).
[22] K. Joulain, J.-P. Mulet, F. Marquier, R. Carminati, J.-J. Greffet, Surf. Sci. Rep. **57**, 59-112 (2005).
[23] S. Basu, Z. M. Zhang, C. J. Fu, International Journal of Energy Research DOI: 10.1002/er.1607
[24] G.A. Domoto, R.F. Boehm and C.L. Tien, J. Heat Transfer **92**, 412 (1970).
[25] C.M. Hargreaves, Phys. Lett. **30A**, 491 (1969).
[26] J. B. Xu, K. Lauger, R. Mller, K. Dransfeld, I.H. Wilson, J. Appl.Phys.**76**, 7210 (1994).
[27] J. B. Xu, K. Lauger, K. Dransfeld, I.H. Wilson, Rev.Sci.Instrum. **65** 2262 (1994).
[28] A. Kittel, W. Müller-Hirsch, J. Parisi, S.A. Biehs, D. Reddig, and M. Holthaus, Phys. Rev. Lett. **95**, 224301 (2005).
[29] U. F. Wischnach, J. Welker, M. Munzel and A. Kittel, Rev. Scientific Instrument **79**, 073708 (2008).
[30] A. Narayanaswamy,S. Shen and G. Chen, Phys. Rev. B **78**, 115303 (2008).
[31] S. Shen, A. Narayanaswamy, G. Chen, Nano Lett. doi: 10.1021/nl901208v (2009).
[32] E. Rousseau, A. Siria, G. Jourdan, S. Volz, F. Comin, J. Chevrier and J-J. Greffet, Nature Photonics DOI 0.1038/NPHOTON.2009.144 (2009)
[33] M. Laroche , R. Carminati, JJ. Greffet. Journ. of Appl. Phys. **100**, 063704 (2006).
[34] W. A. Challener et al., Nature Photonics **3**, 220 (2009).
[35] F. Marquier, K.Joulain, J-P. Mulet, R. Carminati, J-J. Greffet and Y. Chen, Phys. Rev. B **69**, 155412 (2004).
[36] E.D. Palik, *Handbook of optical constants of solids*, Volumes 1-4, Academic Press, New York
[37] C.J. Fu and Z.M. Zhang, Int. Jour. Heat Mass Transfer **49**, 1703 (2006).
[38] N. G. Van Kampen, B. R. A. Nljboer, K. Schram, Phys. Lett. **26**, 307 (1968).
[39] C. Henkel, K. Joulain, J-Ph. Mulet and J-J. Greffet, Phys. Rev. A, **69** 023808 (2004).
[40] M. Abramowitz and I. A. Stegun (ed.) Handbook of Mathematical Functions, National Bureau of Standards, 1964; reprinted Dover Publications, 1965.